Organic template-free synthesis of an open framework silicoaluminophoshate (SAPO) with high thermal stability and high ion conductivity

Dong Fan, Nicolas Barrier, Aurélie Vicente, Jean-Pierre Gilson, Simon Clevers, Valérie Dupray, Gérard Coquerel, Valentin Valtchev

INORGANIC CHEMISTRY FRONTIERS

CCS 中国化学会 CHINESE CHEMICAL SOCIETY

ROYAL SOCIETY OF CHEMISTRY

Organic template-free synthesis of an open framework silicoaluminophoshate (SAPO) with high thermal stability and high ion conductivity

Journal:	*Inorganic Chemistry Frontiers*
Manuscript ID	QI-RES-09-2019-001223.R1
Article Type:	Research Article
Date Submitted by the Author:	29-Oct-2019
Complete List of Authors:	Fan, Dong; Dalian Insititute of Chemical Physics, Barrier, Nicolas; CNRS ENSICAEN, Laboratoire CRISMAT Vicente, Aurelie; LCS, Gilson, Jean-Pierre; ENSICAEN, Laboratory of CATALYSIS & SPECTROCHEMISTRY Clevers, Simon; University of Rouen, SMS Laboratory - UPRES EA 3233 Dupray, Valerie; University of Rouen, Laboratoire SMS Coquerel, Gerard; University of Rouen, SMS Laboratory - UPRES EA 3233 Valtchev, Valentin; Normandie Univ

Organic template-free synthesis of an open framework silicoaluminophoshate (SAPO) with high thermal stability and high ion conductivity

*Dong Fan, [a] Nicolas Barrier,[b] Aurelie Vicente,[c] Jean-Pierre Gilson,[c] Simon Clevers[d], Valerie Dupray[e], Gerard Coquerel[d] and Valentin Valtchev[c]**

[a] National Engineering Laboratory for Methanol to Olefins, Dalian National Laboratory for Clean Energy, Dalian Institute of Chemical Physics, Chinese Academy of Sciences, Dalian 116023, PR China

[b]Normandie Université, ENSICAEN, UNICAEN, CNRS, CRISMAT, 14000 Caen, France.

[c]Normandie Université, ENSICAEN, UNICAEN, CNRS, Laboratoire Catalyse et Spectrochimie, 14000 Caen, France.

[d]University of Rouen, SMS Laboratory - UPRES EA 3233, 76821 Mont-Saint-Aignan, France

[e]University of Rouen, Laboratoire SMS, Centre Universitaire d'Evreux, 27002 Evreux Cedex, France

ABSTRACT

An open-framework silicoaluminophosphate (SAPO) material with a composition of $Cs_2(Al_{0.875}Si_{0.125})_4(P_{0.875}Si_{0.125}O_4)_4(HPO_4)$ was synthesized in an organic template-free cesium-containing system under hydrothermal conditions. The material was resolved to be isostructural with an open-framework aluminophosphate (AlPO) material AlPO-CJ19, which was previously synthesized using pyridine as the solvent and 2-aminopyridine as the organic template via a solvothermal route. The substitution of organic templates by alkaline cations not only makes the current synthesis protocol more favorable from an environmental point of view but also leads to a significantly improved thermal stability of this structure. The framework is kept completely stable at a temperature of 510 ºC. A high-temperature polymorph was discerned at a temperature higher than 540 ºC, the structure of which is revealed to crystallize in *P*1*c*1 space group. UV-vis results reveal that cobalt and copper cations could be readily incorporated through simple ion-exchange treatment. The conductivity of the material is $1.70*10^{-4}$ S cm^{-1} (293K, 30% relative humidity) as revealed by the alternating current (A.C.) impedance spectroscopy analysis. This is the first report of the synthesis of silicon-containing phase with AlPO-CJ19 structure.

Introduction

Open-framework aluminophosphate (AlPO) materials are a family of crystalline materials with uniform pores and channels/cages, which have been widely studied due to their structure diversity and potential applications in catalysis and gas adsorption/separation.[1-4] The open-framework AlPOs could be classified into two categories, according to the electrostatic properties of the associated framework: i) neutral-framework $AlPO_4$ molecular sieves with equal Al and P atoms, and ii) anionic AlPO frameworks with an Al/P ratio differing from of unity. Various framework

Al/P ratios, such as 1/2, 2/3, 3/4, 3/5, 4/5, 5/6, 11/12, 12/13, 13/18, are found for the anionic AlPO compounds.[5-9]

Typically, the synthesis of AlPO materials generally involves the addition of organic compounds as structure-directing agents (SDAs) or templates.[10-13] An obvious drawback of this strategy is the environmental issues, associated with the problematic disposal of the organic containing liquid. Moreover, the high temperature combustion removal of the organic templates is an energy intense process. Besides, the structures of the anionic AlPO could be damaged upon the calcination removal of the occluded organic template. Consequently, to develop an environment benign and low-cost organic-free synthesis route is highly desirable for the practical applications of AlPOs. Although various aluminosilicate zeolites, including FAU,[14] ABW,[15] LEV,[16] Beta,[17-18] ZSM-34,[19-21] FER,[22] EMT,[23-24] *etc.*,[25-26] are synthesized by employing alkali/alkali earth cations or by seed-induced approaches, examples of successful AlPO crystalline materials without recourse to organic template remains rare. Continuous efforts have been devoted to the organic-free synthesis of AlPO materials.[15, 27-33] Wang *et al.* developed an organotemplate-free method for the synthesis of zeolitic materials in the Al_2O_3–P_2O_5–Na_2O–H_2O system, and an AlPO material of AEN zeotype structure with the nominal composition of $Na(H_2O)_2|[(AlPO_4)_3OH$ was prepared.[32] Afterwards, the synthesis of a new magnesium aluminophosphate JU102 with chiral structures was achieved using a similar strategy.[31] By adjusting the synthesis gels and conditions, the same group also succeeded in synthesizing another new open-framework aluminophosphate: $Na_6[(AlPO_4)_8(OH)_6].8H_2O$, which possesses excellent proton conductivity.[30] Very recently, Hong *et al.* successfully synthesized a variety of SAPO molecular sieves of high framework charge densities, including MER, EDI, GIS, and ANA type structures, in hydrogels containing different types and concentrations of alkali metal cations without recourse to OSDAs,[28] although some of the these

phosphate zeolites have also been seen by Flanigen and Grose with alkali cations in the early 1970s.[33]

In this work, a novel SAPO material is successfully synthesized in a Cs^+ containing hydrogel. The chemical formula of this material is $Cs_2(Al_{0.875}Si_{0.125})_4(P_{0.875}Si_{0.125}O_4)_4(HPO_4)$. The structure of this material is revealed to be iso-structural with $(NH_4)_2Al_4(PO_4)_4(HPO_4)\cdot H_2O$ (AlPO-CJ19),[34] a previously reported aluminophosphate material synthesized using solvothermal synthesis route, in which pyridine was used as the solvent and 2-aminopyridine as the SDA. From an environmental point of view, the substitution of the organic template by inorganic Cs ions makes the current synthesis protocol more favorable. Moreover, the incorporated Cs^+ endows the material with improved thermal stability and high proton/ion conductivity.

Experimental Section

Material Synthesis

The SAPO material was synthesized using an organic-free method. The employed molar composition of the gel is: $2.2CsOH: 1SiO_2: 1Al_2O_3: 2.0P_2O_5: 120H_2O$. Ultra-stable Y (US-Y) zeolite (CVB720), purchased from Zeolyst and zeolite L zeolite, purchased from Tosoh, is used as silica-alumina source. Prior to the synthesis, zeolite L was subjected to dealumination using 1 M HNO_3 acid solution. The solid:liquid ratio was 1:40. The zeolite was treated at room temperature for 6 h, then thoroughly washed with distilled water and dry. Aluminum metal powder and phosphoric acid are chosen as the aluminum and phosphor sources, respectively. A typical synthesis procedure using US-Y includes: i) 0.25 g USY with a Si/Al ratio of 18.7 was added into 10 grams of CsOH solution (1 M) and the slurry was put under agitation for 1 h; ii) 0.216 gram of Al metal powder was added gradually to the slurry and the agitation continued until the total

reaction dissolution of the Al metals; iii) 3.2 grams of phosphoric acid solution (50 wt%) was subsequently added drop wise. The synthesis procedure based on HNO_3-treated L zeolite is similar. The synthesis with USY (Si/Al=18.7) and dealuminated zeolite L (Si/Al=781) were all performed at 180°C for 72 h. The resultant solid product is collected and washed thoroughly with distilled water. The samples obtained from the USY and HNO_3-treated L zeolite containing system were denominated DFZ-64C and DFZ-64D, respectively.

Characterizations

The powder X-Ray diffraction (PXRD) data were measured on a Bruker D8 advance vario1 diffractometer equipped with primary germanium (111) Johansson monochromator ($\lambda K\alpha 1$ = 1.5406 Å) and a Lynx Eye detector. A PXRD diagram was recorded at room temperature between 5 and 130°(2θ) with a step of ~0.009°(2θ) and a time of 4.7 s per step. We also used a variable divergent slit for a constant illuminated sample length of 4 mm. Temperature-dependent powder X-ray diffraction (TD-PXRD) data were recorded on the same diffractometer with an Anton Paar HTK1200N chamber, under air atmosphere, every 30°C until 720°C. Each diagram was recorded with a constant illuminated length of 6 mm, between 7.5 and 60°(2θ) with a step of ~0.014°(2θ).

Temperature resolved second harmonic (TR-SHG) measurements were recorded with the following equipment. A Nd:YAG Q-switched laser (Quantel) operating at 1.06 μm was used to deliver up to 360 mJ pulses of 5 ns duration with a repetition rate of 10 Hz. An energy adjustment device made up of two polarizers (P) and a half-wave plate ($\lambda/2$) allowed the incident energy to vary from 0 to ca. 300 mJ per pulse. A RG1000 filter was used after the energy adjustment device to remove the light from laser flash lamps. The samples (few mg of powder in a crucible) were placed in a computer-controlled Heating-Cooling stage (Linkam THMS-600) and were irradiated

with the laser beam (4 mm in diameter). The signal generated by the sample (diffused light) was collected into an optical fiber (500 μm of core diameter) and directed onto the entrance slit of a spectrometer (Ocean Optics). A boxcar integrator allowed an average spectrum (spectral range 490-590 nm) with a resolution of 0.1 nm to be recorded over 3 s (30 pulses). The incident energy was set at circa 200mJ. For temperature resolved measurements, the SHG response was recorded between 20 and 500° C with a heating rate of 1° C/min.

The one-dimensional (1D) ^{27}Al and ^{31}P magic-angle spinning nuclear magnetic resonance (MAS NMR) measurements were performed on a Bruker Advance 500 MHZ spectrometer using 4 mm ZrO_2 rotors. The ^{27}Al MAS NMR spectra were recorded under quantitative conditions at a ^{27}Al frequency of 130.29 MHz using a short pulse length of 0.77 μs with an rf field of *ca.* 23 kHz, corresponding to the non-selective flip angle of *ca.* π/12, a spinning rate of 12 or 14 kHz and a recycle delay of 1 s. The ^{27}Al chemical shifts are reported relative to 1.0 M $Al(H_2O)_6^{3+}$ solution. The ^{31}P MAS NMR spectra were measured at 130.29 MHz with a pulse length of 5.0 ms, a recycle delay of 60 s and the addition of about 3000 pulse transients. ^{1}H-^{31}P cross polarization (CP) MAS NMR spectroscopy was carried out with a contact time of 3 ms and a recycle delay of 2 s. The ^{31}P chemical shift is reported relative to 0.1 M H_3PO_4. All 1D NMR spectral decomposition and simulation were performed using the PeakFit curve-fitting program. The two-dimensional (2D) ^{27}Al multiple-quantum (MQ) MAS NMR spectra were recorded at 104.26 MHz on a Bruker Avance 400 spectrometer (9.4 T) using a 4 mm MAS probehead. The MAS NMR spectra were recorded using a pulse length of 1.3 ms with an rf field of *ca.* 30 kHz, corresponding to the non-selective flip angle of *ca.* p/12, and a recycle delay of 0.2 s. For MQ MAS, the multiplex spam z-filter pulse method was used as it was shown to produce fast and high-quality spectra. The detailed procedure used in this method was described elsewhere.[35-36] The initial excitation and conversion

hard pulse lengths were 2 and 0.8 ms with an rf field of 160 kHz, respectively. The soft pulse was 9 ms with a *rf* field of 30 kHz.

Elemental compositions were measured by inductively coupled plasma–atomic emission spectroscopy (ICP-AES) using an OPTIMA 4300 DV (Perkin– Elmer) instrument. A MIRA-LMH (Tescan) scanning electron microscope equipped with a field emission gun was employed to obtain the SEM images. TGA/DTA measurements of the samples were carried out using a SETSYS 1750 CS evolution instrument (SETARAM). 15 mg of the sample was heated from 25 to 800 °C with a ramp rate of 5 ° C min-1 under air atmosphere (flow rate: 40 mL min^{-1}). In-situ temperature-dependent Fourier transform infrared (FTIR) analyses were carried out on a NICOLET 5700 FT-IR spectrometer equipped with an TGS detector. The self-supporting disk (20 mg, 15mm in diameter) of the sample was placed in an IR cell attached to a conventional vacuum system. The IR spectra were recorded on the sample after thermal treatment at different temperatures with 128 scans at 4 cm^{-1} of the resolution. UV-vis absorption spectra of the cobalt and copper exchanged zeolite powders were recorded using a Varian Cary 4000 Spectrophotometer.

A.C. Impedance Spectroscopy. The as-synthesized powder was pressed into self-supporting disk under a force of 1 MPa. Then the sample disk was sealed with the shells of CR2016 coin cells. Electrochemical impedance spectroscopy (EIS) of the coin cell was scanned from 1.0×10^6 to 1.0×10^4Hz at open-circuit voltage with an amplitude of 10 mV on Solartron 1287 and Solartron 1260 electrochemical stations. Therefore, the ionic conductivity of the sample (σ) was calculated by the ohmic resistance of coin cell (R) and the calculation equation: σ=l/RA, where the l and A stand for thickness and surface area of the sample plate, respectively. It is notable that the ohmic resistance of coin cell was obtained by fitting with a Zview software, and the thickness and surface area of the sample plate was measured as 0.16 cm and 2.0 cm^2, respectively.

Results and discussion

A crystalline phase with well-resolved XRD diffractions is prepared from the reaction mixture with an optimal composition of 2.2CsOH: 1SiO_2: 1Al_2O_3: 2.0P_2O_5: 120H_2O (Figure 1). All peaks are well resolved, revealing the good crystallinity of the material. No halo due to the existence of amorphous residues could be discerned in the XRD patterns.

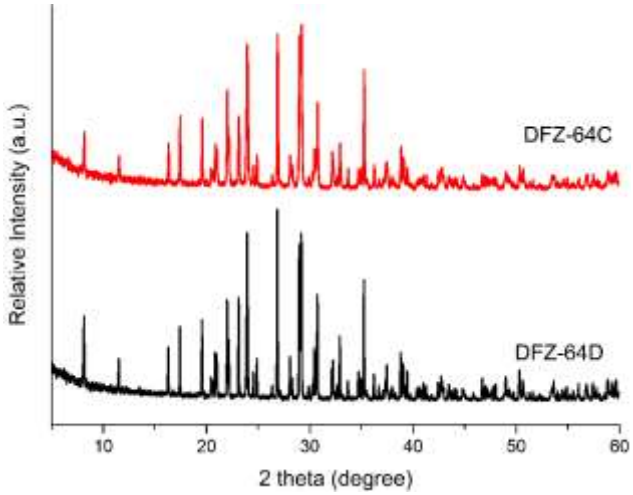

Figure 1 XRD patterns of the as-synthesized samples

SEM images of the prepared SAPO materials are presented in Figure 2. Two morphologies could be observed for the synthesized samples. DFZ-64D synthesized using HNO_3-treated LTL zeolite as the silicon source possesses the morphology of flower-like assemblies, the size of which locates in the range of 50 to 80 μm. For DFZ-64C synthesized using ultra-stable Y as the silicon sources, the size of the aggregates is reduced to 5 - 10 μm, suggesting that the choice of Si source is crucial in controlling the morphologies of this material. This might be due to the different Si incorporation degree of the two samples. The elemental compositions of the two as-synthesized samples are determined by ICP-AES analysis. And the elemental compositions are calculated to be $Cs_{0.17}Al_{0.32}P_{0.38}Si_{0.13}$ for DFZ-64C and $Cs_{0.20}Al_{0.33}P_{0.43}Si_{0.05}$ for DFZ-64D. The preferred

crystallization temperature is 180 ºC. The crystallization could be carried out under either static or tumbling conditions. When the crystallization is carried out at lower temperatures, only a dense phase without well-defined crystalline structures is obtained.

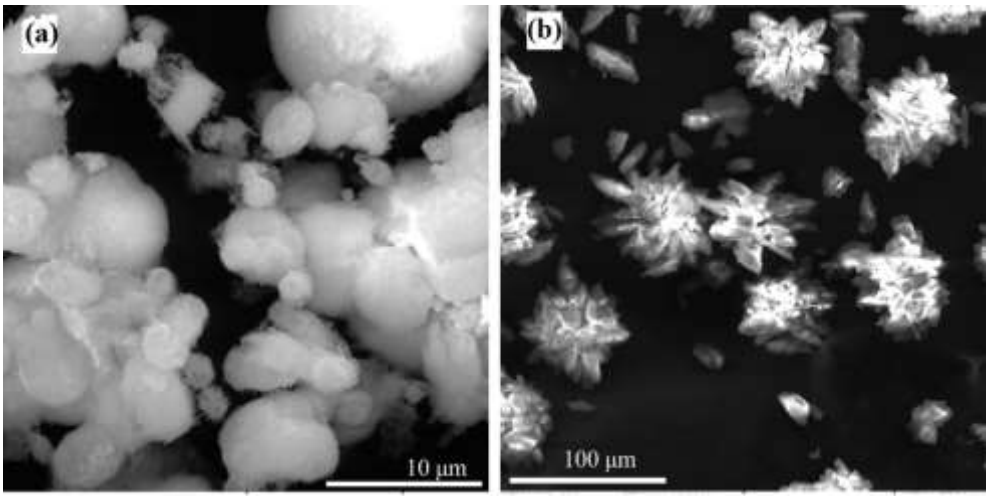

Figure 2 SEM images of the as-synthesized samples DFZ-64C (a) and DFZ-64D (b).

Structure analysis

The PXRD diagram of DFZ-64C-LT at 20ºC (the low-temperature (20ºC) form of DFZ-64C, Figure 3) was indexed with the program DICVOL06[37] in an monoclinic unit cell with the following parameters: a = 5.09051(1) Å, b = 21.75661(6) Å, c = 8.22408(2) Å, β = 90.4280(2)°. A whole profile matching of the PXRD diagram was performed with the JANA2006 program[38-39] with the $P2$ space group. A careful observation of the extinction conditions evidences the $P2_1$ or $P2_1/m$ space groups. A Second Harmonic Generation (SHG) qualitative test was performed on a white powder sample of DFZ-64C, in reflection configuration. A notable SHG signal was observed, which proved that the crystal structure of this compound is non-centrosymmetric[40]. The structure was then solved *ab initio* with the SUPERFLIP program[41] which gave a solution in the non-centrosymmetric space group $P2_1$. A first model was obtained without Si atom. The Rietveld refinements were performed with the JANA2006 program with fundamental parameter approach.

The preferential orientation along the [010] direction was taken into account assuming the March & Dollase function. All the atomic positions and isotropic displacement parameters (U_{iso}) were refined. The bond valence sums (BVS)[42] calculated with parameters provided by Brese and O'Keeffe[43] showed a lack of electronic charge on the O2 atom. This indicated the presence of a hydrogen atom bonded to O2. This hydrogen atom was geometrically added with distance and angle restraints. There was also a lack of electronic charge on the P5 and an excess of electronic charge on the Al3 atom positions. Mixed 0.5P/0.5Si and 0.5Al/0.5Si occupancies were taken into account for the P5 and Al3 positions, which corresponded to the expected chemical formula $Cs_2(Al_{1-x}Si_x)_4(P_{1-x}Si_xO_4)_4(HPO_4)$ with x = 0.125. Nevertheless, if the mixed occupancy 0.5P/0.5Si of the "P5" position is quite sure, it can be excluded that the other Si amount is statistically spread over all Al crystallographic sites. The final reliability factors obtained after the last refinement cycle are: R_{Fobs} = 3.19% and R_{wp} = 4.35%. All refinement and crystallographic parameters of DFZ-64C are summarized in Table 1. The atomic positions, the U_{iso} parameters and the bond valence sums (BVS)[42] are presented in the supplementary Table S1. A selection of interatomic distances of DFZ-64C is shown in Table 2.

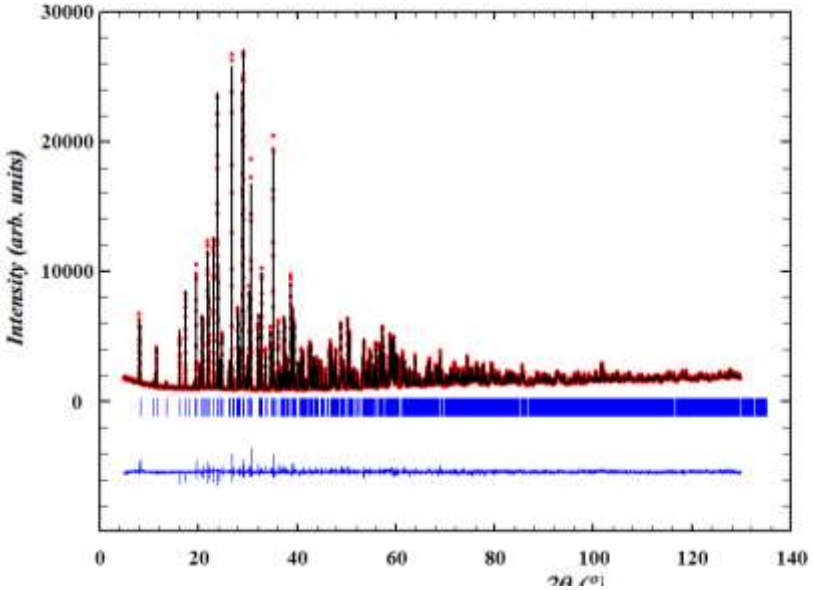

Figure 3 PXRD diagram of DFZ-64C-LT at 20ºC (Cu–Kα1 radiation; 1.5406Å) with observed (dots), calculated (solid line), Bragg reflections (ticks), and difference profiles (bottom line) obtained after Rietveld refinements.

Table 1. Details of PXRD diagrams and Rietveld refinements of DFZ-64C-LT at 20ºC and DFZ-64C-HT at 570ºC (the high temperature form (20ºC) of DFZ-64C)

Diffractometer	Bruker D8 advance vario1		
Radiation (Å)	Cu-Kα_1 radiation λ = 1.5406		
Temperature (°C)	**20**	**570**	
2θ-range / step (°)	5 – 129.997 / ~0.009	10 – 126.181 / ~0.012	
Phase	**DFZ-64C-LT**	**DFZ-64C-HT**	**$AlPO_4$**
Space Group	*P*12$_1$1	*P*11*b*	*P*63*mc*
Z	2	2	2
a (Å)	5.093345(13)	5.13528(5)	5.10028(4)
b (Å)	21.76885(5)	21.8182(2)	5.10028(4)
c (Å)	8.22861(2)	8.29896(9)	8.3375(7)
β (°)	90.4280(2)	89.327(1)	
V /Å^3	912.332(4)	929.77(2)	
Molar mass (g.mol^{-1})	848.7	848.7	
Mass concentration (%)	100	96.8(1)	3.2(1)
Rietveld refinement:			
Shape	Pseudo-Voigt	Pseudo-Voigt	
Background	10 Legendre polynoms	20 Legendre polynoms	
Preferred orientation	March & Dollase ; *b*-axis	March & Dollase; *c*-axis	
Asymmetry	Fundamental parameter	Fundamental parameter	
Anisotropic reflection broadening	-	Stephens	
Rietveld agreement indices			
R_{Fobs}	0.0320	0.0361	0.0515
R_{Bobs}	0.0547	0.0583	0.0983
*Rw*p	0.0436	0.0492	
*cR*wp	0.1051	0.1451	
Gof	1.83	2.18	

Table *2*. Selected interatomic distances for DFZ-64C-LT at 20 ºC and DFZ-64C-HT at 570 ºC (both polymorphs of $Cs_2(Al_{0.875}Si_{0.125})_4(P_{0.875}Si_{0.125}O_4)_4(HPO_4)$).

Atom 1	Atom 2	Distances (Å)		Atom 1	Atom 2	Distances (Å)	
		DFZ-64C-LT	DFZ-64C-HT			DFZ-64C-LT	DFZ-64C-HT
Al1	O10	1.90(1)	1.77(3)	P1	O10	1.48(1)	1.44(3)
	O12	1.85(1)	1.70(3)		O12	1.52(1)	1.70(3)
	O13	1.92(1)	2.16(3)		O18	1.58(1)	1.59(3)
	O4	1.81(1)	1.92(3)		O9	1.61(1)	1.66(2)
	O7	1.87(1)	1.92(3)	P1-O average		1.55	1.60
	O8	1.95(1)	1.96(3)	P2	O1	1.59(1)	1.84(3)
Al1-O average		1.88	1.91		O11	1.55(1)	1.47(3)
Al2	O16	1.86(1)	1.83(3)		O15	1.49(1)	1.16(3)
	O19	1.77(1)	1.78(3)		O5	1.48(1)	1.46(3)
	O3	1.83(1)	1.84(3)	P2-O average		1.53	1.48
	O5	1.88(1)	1.96(3)	P3	O13	1.51(1)	1.54(3)
	O9	1.78(1)	1.74(3)		O16	1.48(1)	1.49(3)
Al2-O average		1.82	1.83		O2	1.65(1)	1.73(2)
Al/Si3	O1	1.68(1)	1.48(3)		O7	1.43(1)	1.36(3)
	O14	1.74(1)	1.75(3)	P3-O average		1.52	1.53
	O15	1.78(1)	2.17(3)	P4	O14	1.61(1)	1.50(3)
	O17	1.67(1)	1.63(2)		O19	1.54(1)	1.56(2)
Al/Si3-O average		1.72	1.76		O3	1.51(1)	1.58(3)
Al4	O11	1.76(1)	1.79(3)		O8	1.51(1)	1.58(2)
	O18	1.76(1)	1.59(3)	P4-O average		1.54	1.56
	O20	1.76(1)	1.68(3)	P/Si5	O17	1.57(1)	1.52(2)
	O6	1.72(1)	1.94(3)		O20	1.59(1)	1.57(3)
Al4-O average		1.75	1.75		O4	1.61(1)	1.57(2)
					O6	1.56(1)	1.45(3)
				P/Si5-O average		1.58	1.53

The structure projection of DFZ-64C is shown in Figure 4. Sample DFZ-64C is revealed to be isostructural with $(NH_4)_2Al_4(PO_4)_4(HPO_4)\cdot H_2O$. Both structures correspond to an open framework base on $[AlO_4]$, $[AlO_5]$, $[AlO_6]$, $[PO_4]$ and $[PO_3OH]$ polyhedra. Compared with $(NH_4)_2Al_4(PO_4)_4(HPO_4)\cdot H_2O$, the charge of macro-anion $[(Al_{4-x}Si_x)(P_{1-x}Si_xO_4)_4(HPO_4)]^{2-}$ for DFZ-64C is counterbalanced by two Cs^+ cations. On the four crystallographic Al positions, Al4 and the mixed Al/Si3 atoms are in tetrahedral coordination $[(Al/Si)O_4]$. The Al-O distances for

Al4 range between 1.72(1) and 1.76(1) Å with an average distance of 1.75 Å, which is the same as the one in $(NH_4)_2Al_4(PO_4)_4(HPO_4).H_2O$. For Al/Si3 the Al-O distances range between 1.67(1) and 1.78(1) Å. The corresponding average distance of 1.72 Å is comparable to that of 1.74 Å observed in $(NH_4)_2Al_4(PO_4)_4(HPO_4)\cdot H_2O$ with a difference of 0.02 Å. The two remaining Al atoms are in trigonal pyramid coordination [$Al2O_5$] (Al-O bond distances: 1.77(1)-1.88(1) Å) and in octahedral coordination [$Al1O_6$] (Al-O bond distances: 1.81(1)-1.95(1) Å). The respective average distances $d_{Al\text{-}O\text{-}moy}$ are 1.82 and 1.88 Å, in accordance with those in $(NH_4)_2Al_4(PO_4)_4(HPO_4)\cdot H_2O$ of 1.83 and 1.90 Å. All [AlO_x] polyhedra are isolated from each other by the [PO_4] tetrahedra with which they share O atoms. All the P atoms are in tetrahedral coordination [PO_4]. The tetrahedra of the P1, P2, P4, and P5 atoms share all O apex with adjacent Al atoms. For the P/Si5 mixed atom, the P/Si-O distances range between 1.56(1) and 1.61(1) Å with an average distance of 1.58 Å, which is 0.05 Å bigger than the one in $(NH_4)_2Al_4(PO_4)_4(HPO_4)\cdot H_2O$. For P1, P2 and P4 (P-O bond distances: 1.48(1)-1.6(1) Å), the average P-O distances are 1.55, 1.53 and 1.54 Å, respectively, in agreement with the values observed in $(NH_4)_2Al_4(PO_4)_4(HPO_4)\cdot H_2O$ (1,53, 1,53 and 1,52 Å). The [$P3O_4$] tetrahedra share two O apexes with Al1 (P3-O bond distances: 1.43(1) and 1.51(1) Å) and one O apex with Al2 (P3-O16 bond length: 1.48(1) Å). The last O apex corresponds to a terminal OH- group, which points to the center of one of the two eight-sided tunnel (P3-O2 bond length: 1.65(1) Å). Both tunnels are delimited by an alternation of [AlO_x] and [PO_4] polyhedra in the (*bc*) plane. The two Cs^+ cations reside in these tunnels merely with weak van der Waals interactions, since the smallest Cs-O distances are calculated to be 3.06(1) Å for Cs1 and 3.10(1) Å for Cs2.

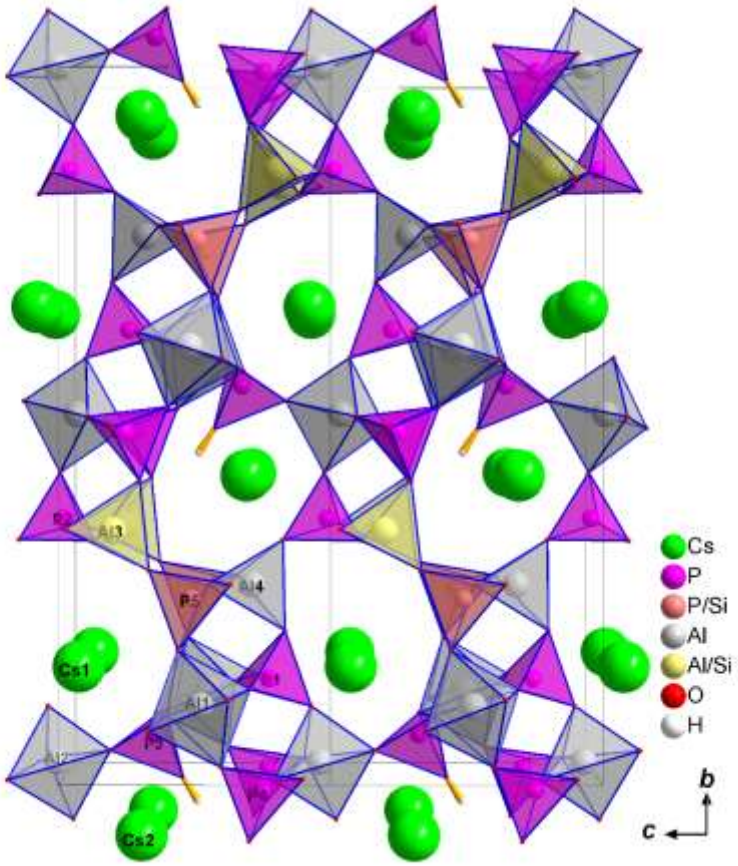

Figure 4 Structure projection of the *(bc)* plane; 8-MR channels occupied by Cs^+ cations are observed along the *a* axis.

The coordination status of the framework species of DFZ-64C is further probed using MAS NMR techniques (see Figure 5). The ^{27}Al MAS NMR spectra exhibit three resonance peaks at 42.5, 10 and -17.5 ppm, which could be assigned to tetra-, penta- and hexa- coordinated [AlO_4], [AlO_5] and [AlO_6] species, respectively. Deconvolution results reveal that the relative content of the [AlO_4], [AlO_5] and [AlO_6] is in an approximate ratio 2/1/1. Note that the second-order quadrupolar interactions experienced by the half-integer quadrupolar nuclei could alter the resonance signals in the 1d ^{27}Al MAS NMR spectra. The 2D MQ MAS technique was employed to eliminate the second-order quadrupolar interaction and the corresponding spectra are presented

in Figure 5. In the isotropic (F1) dimension, four peaks could be unambiguously identified. The two peaks with relatively lower chemical shifts correspond to the [$Al2O_5$] and [$Al3O_6$] species, which is congruent with the 1d Al MAS results. The adjacent two peaks at higher chemical shifts in the F1 dimension should be ascribed to the tetracoordinated [AlO_4] species at different crystallographic Al sites. This is in good congruence with the structure solution results in the previous sector, which shows that two crystallographic sites co-exist for the tetra-coordinated Al1 species and mixed Al/Si4 sites.

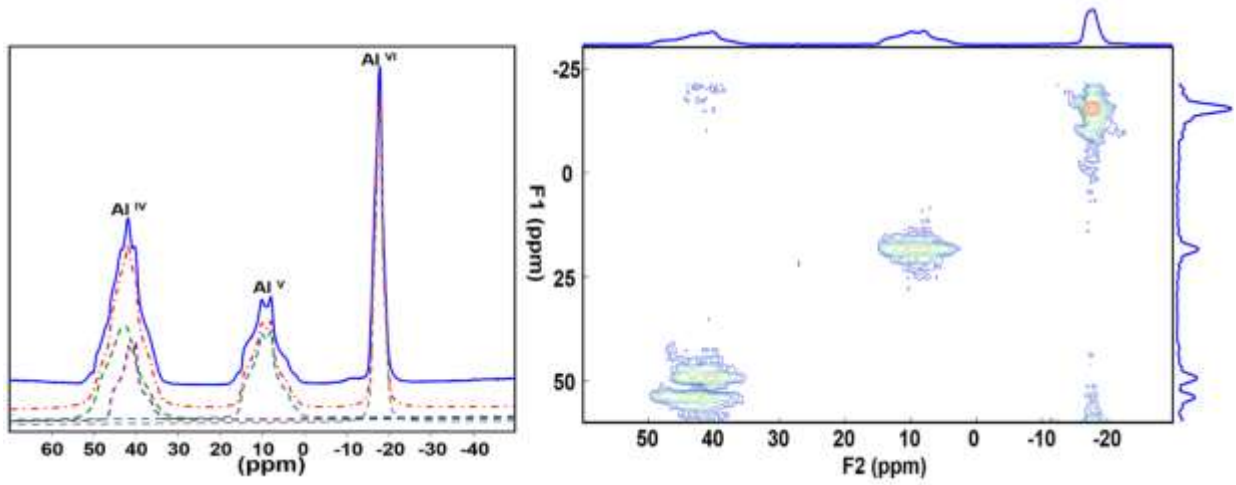

Figure 5 1d ^{27}Al MAS NMR spectra (left) and 2d ^{27}Al MQ MAS NMR spectra (right) of sample DFZ-64C

The phosphorus atom coordination environments are probed by *^{31}P MAS NMR* technique and the corresponding spectrum is shown in Figure 6. The deconvoluion of the spectrum reveals that the curve comprises five independent resonance peaks, centered at -21.7, -22.7, -25.1, -26.7 and -29.5 ppm, which corresponds to the tetragonal [PO_4] species at the five crystallographic phosphor sites, respectively. Moreover, the relative ratio of the five tetragonal [PO_4] species is calculated to be around 0.23:0.21:0.16:0.24:0.17. The deviation from unity might be explained by the fact that in some position P is partially replaced with Si, which is also well supported by the crystallographic

analysis. *^{1}H-^{31}P CP MAS NMR* spectrum of the sample is also collected and shown in Figure 6. The resonance peak at -21.7 ppm is significantly enhanced in the CP MAS spectra, indicating that the peak at -21.7 ppm corresponds to the P5 site linked with the terminal hydroxyl groups revealed in the structure analysis results.

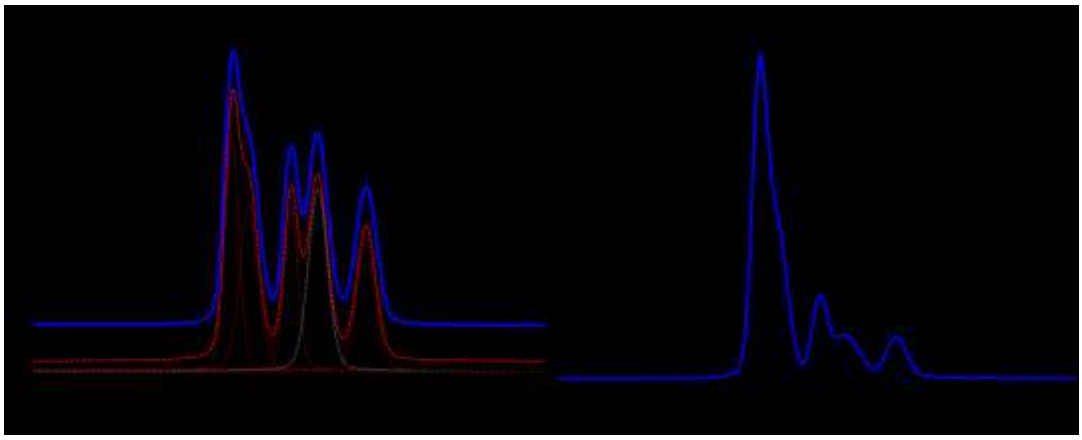

Figure 6 ^{31}P MAS (left) and ^{1}H-^{31}P CP MAS NMR spectra (right) of sample DFZ-64C.

Thermal Stability

Thermal stability is an important property influencing the potential applications of the open-framework aluminophosphate materials. As mentioned in the XRD analysis, the XRD patterns of the material show no significant variation after calcination at 550 ºC. This phenomenon is quite different from its aluminophospahe counterpart $(NH_4)_2Al_4(PO_4)_4(HPO_4)\cdot H_2O$, denoted as AlPO-CJ19 [34]. A comprehensive analysis is further carried out to investigate the thermal behavior and phase transformation phenomenon of material, using combined technologies of TG-DSC, temperature-programed *in-situ* XRD and *in-situ* temperature-dependent FTIR analysis.

TGA curve reveals a continuous weight loss of merely 1.8 wt% from room temperature to around 600 ºC, due to the thermal desorption of the incorporated water molecules. This is quite different from the typical TGA curves of the organic-incorporated aluminophosphate materials, for which significant weight losses due to the combustion removal of the occluded organics are generally

observed. In fact, the weight loss curve between 200 to 600ºC is clearly composed of two different weight losses (before and after 400ºC), corresponding to the removal of the weakly bonded and strongly bonded water molecules, respectively. Another notable weight loss of around 1wt% is observed in the temperature range between 600 and 700 ºC (also evidenced by the presence of the sharp peak in the DTG curve), accompanied by an obvious endothermic peak. This weight loss is associated with the framework collapse and decomposition of the material.

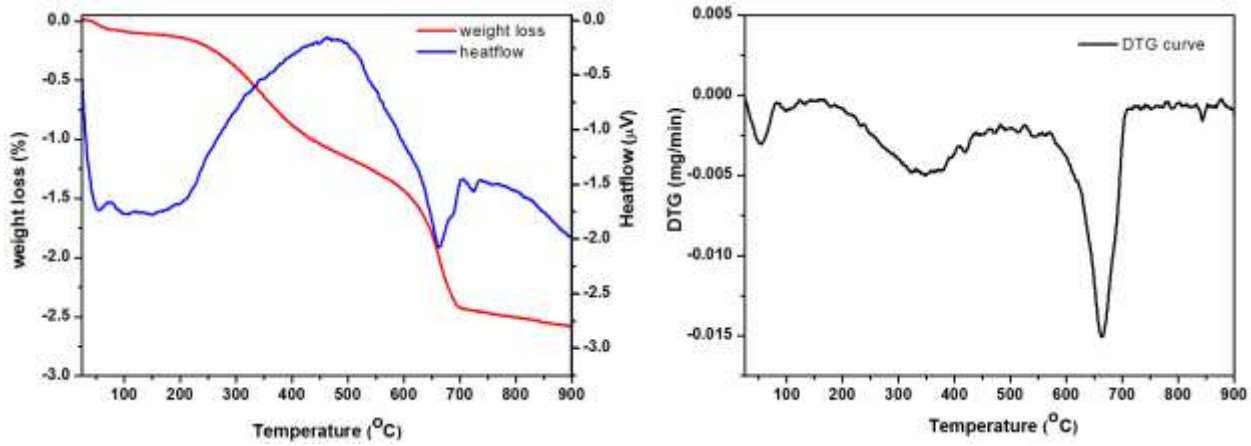

Figure 7 TG-DSC analysis curves of sample DFZ-64C: TGA and heat flow curves (left) and DTG curve (right).

The phase transition of the sample is monitored by the temperature-programmed *in-situ* XRD analysis and the corresponding XRD patterns are shown in Figure 8. Below 510 °C, the positions and intensities of the XRD patterns show no variation, suggesting that the structure of the framework is rather stable and barely perturbed by the thermal treatment below 510 °C. However, upon increasing the temperature to 540 ºC, a phase transition between two polymorphs of $Cs_2(Al_{0.875}Si_{0.125})_4(P_{0.875}Si_{0.125}O_4)_4(HPO_4)$ is evidenced. For clarity, the two polymorphs are denoted as DFZ-64C-LT for the low-temperature form and DFZ-64C-HT for the high-temperature form, respectively. The structures of both polymorphs (DFZ-64C-LT at 510ºC and DFZ-64C-HT at 570ºC) are resolved and depicted in Figure 9. Both structures are monoclinic: the phase DFZ-

64C-LT at 510ºC crystallizes in the $P2_1$ space group and its high temperature counterpart crystallizes in $P11b$. This non-conventional setting was chosen to conserve the same *a*, *b* and *c*-axis for both structures. Again, a notable SHG signal was observed at 540°C, which proved that the crystal structure of this HT-phase is also non-centrosymmetric (Figure S3). Both space groups are polar and non-centrosymmetric but there are no group-subgroup relations between the two structures meaning this transition is of first-order. The structure was solved *ab initio* against PXRD data at 570°C in the P11b space group with the SUPERFLIP program. Rietveld refinements were performed with JANA2006. (Fig s2) Anisotropic peak broadening was taken into consideration using the Stephens model[44]. Indeed, the phase transformation implies a strong compression along the *b*-axis which decrease from 21.9 Å at 510°C to 21.8190(2) Å at 570°C (Fig 10). In parallel β goes to 90° while γ is reduced from 90 to 89.3276°. This strong anisotropic strain in phase $Cs_2(Al_{0.875}Si_{0.125})_4(P_{0.875}Si_{0.125}O_4)_4(HPO_4)$-HT, also explains the decreasing of the SHG signal (see Figure s1). Note that the sample also undergoes a slight decomposition with the appearance of the $AlPO_4$ phase during the phase transition. All refinement and crystallographic parameters of DFZ-64C-HT at 570ºC are summarized in Table 1. The atomic positions and the Uiso are presented in Table 2. A selection of interatomic distances of DFZ-64C-HT at 570ºC is shown in Table 2. Finally, after the temperature is above 600 ºC, the sample decomposes into SiO_2, $AlPO_4$, and $CsPO_3$, which is congruent with the TG-DSC results revealing that occurrence of the framework decomposition in the same temperature range.

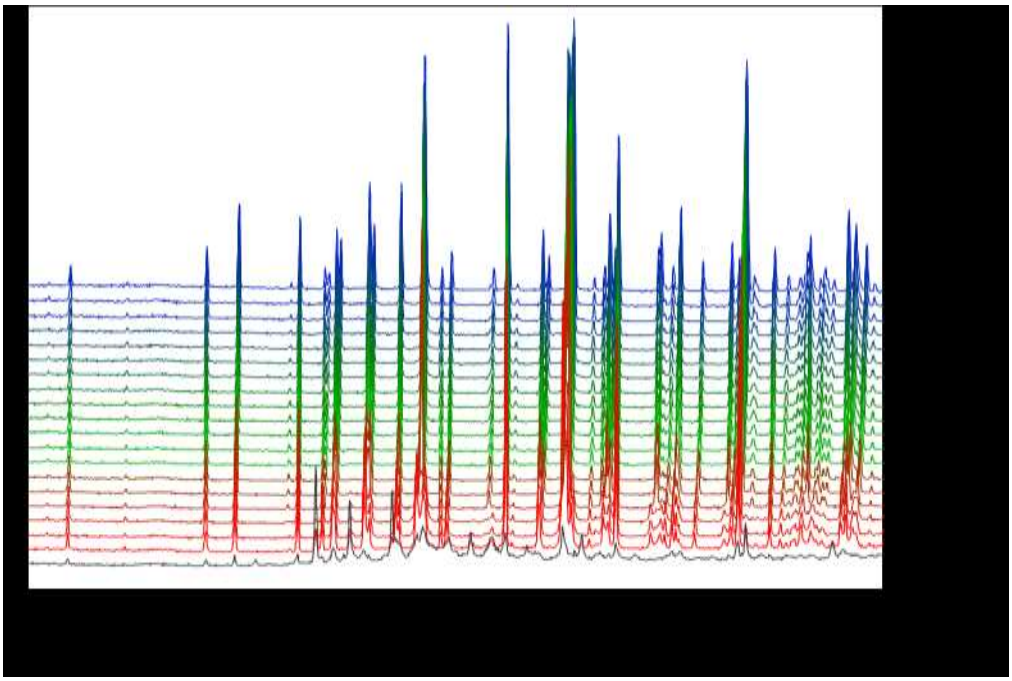

Figure 8 Temperature-programmed in-situ XRD patterns of sample DFZ-64C.

If one compares the structures of two polymorphs just before and above the transition at 510 and 570°C (Figure 9) it can be seen that the open framework based on [AlO_4], [AlO_5], [AlO_6], [PO_4] and [PO_3OH] polyhedral is conserved. The loss of the 2_1 axis along the *b*-axis replaced by the *b* glide-plan perpendicular to the *c*-axis. This transformation essentially traduces by oxygen atom displacements while the cations stay roughly on the same positions. All average P-O and Al-O distances in DFZ-64C-HT at 570ºC are comparable to those observed previously in DFZ-64C-LT at 20ºC. (Table 2).

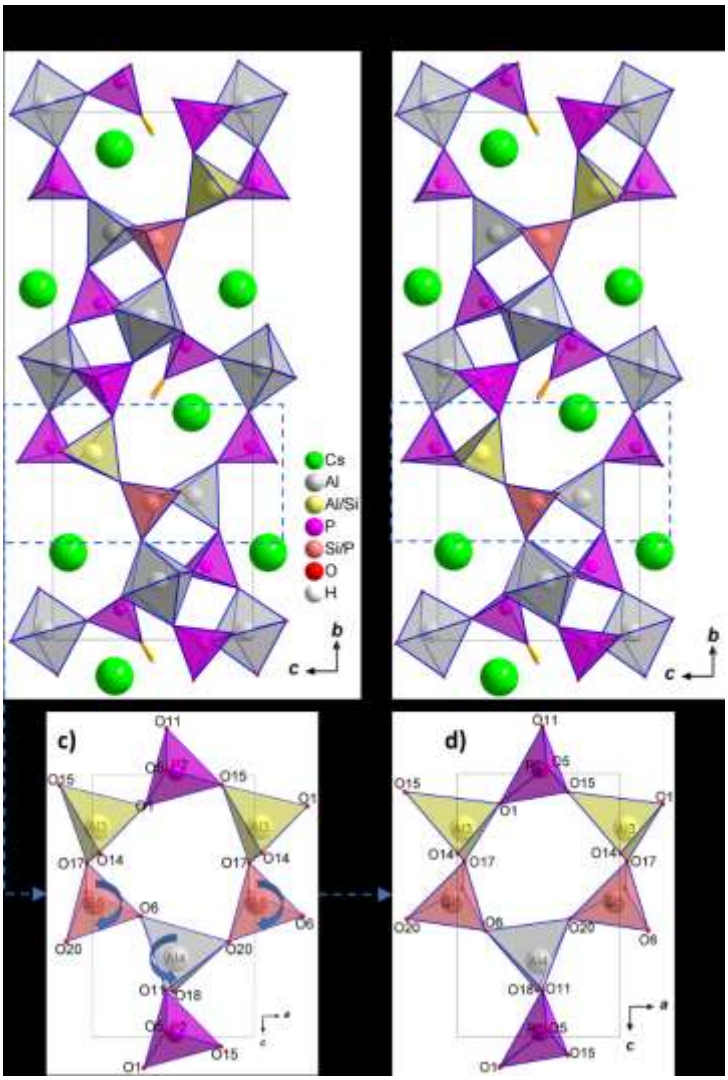

Figure 9 Views of the structures of $Cs_2(Al_{0.875}Si_{0.125})_4(P_{0.875}Si_{0.125}O_4)_4(HPO_4)$ polymorphs a) DFZ-64C-LT at 510°C and b). DFZ-64C-HT at 570°C after the transition. Bottom, figures c) and d) show the displacement of the oxygen atoms between the two polymorphs for part of the structural framework. The blue arrows in the LT structure indicate how the $[Si5O_4]$ and $[Al4O_4]$ tetrahedra must rotate around the b axis to form the HT structure.

The hydroxyl functional groups are of particular interests for the applications of porous material. *In-situ* FTIR techniques are used to identify and follow the variation of the -OH groups with the ramp of temperature (Figure 10). Four absorptions at around 3743, 3659, 3571 and 3456 cm^{-1}

could be observed. The peak at 3743 cm^{-1} is ascribed to the hydroxyls attached to the crystal surfaces. The peaks at 3659 and 3571 cm^{-1} are speculated to arise from water molecules weakly hydrogen-bonded to the aluminum and phosphor species in the defect sites. With the increase of temperature, the intensities of the two peaks diminish gradually and disappear completely above 350 ºC, suggesting the complete removal of the weakly adsorbed water molecules, which corresponds well to the first weight loss in the TG analysis. The hydroxyls corresponding to the absorption peak at 3456 cm^{-1} is rather stable. Below 450 ºC, no significant decrease in the peak at 3456 cm^{-1} could be discerned. After thermal treatment at 550 ºC, only a tiny decrease could be observed. These hydroxyls with relatively higher thermal stability are speculated to correspond to the -OH groups linked with the framework P species at P5 sites, as revealed by the XRD refinement analysis.

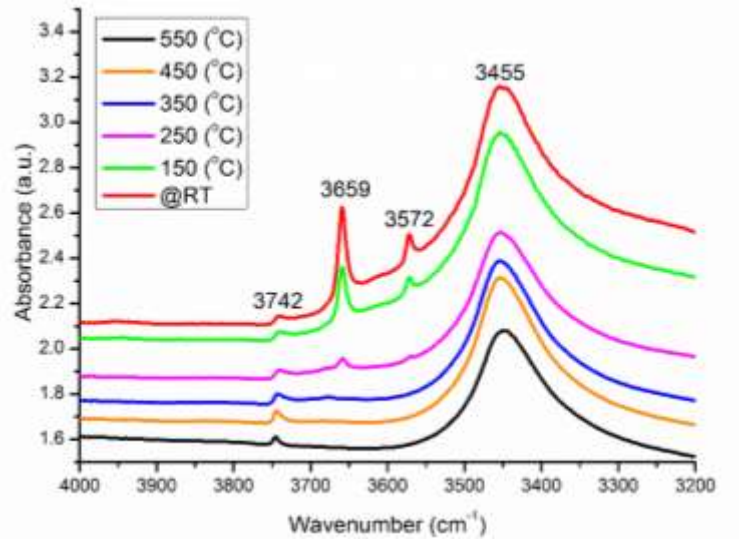

Figure 10 Analysis of the -OH stretching mode of sample DFZ-64C by temperature-programmed in-situ FTIR spectroscopy.

Ion-exchange Properties

The UV-vis absorption spectra of cobalt and copper exchanged samples are shown in Figure 11. In the spectra of Co^{2+} exchanged sample, an absorption peak centered at the wavelength of 526

nm could be observed, which corresponds to the isolated octahedral Co^{2+} cations introduced during the ion exchange process. The light pink color of the powder also suggests that the majority of the exchanged Co^{2+} are in the octahedral coordination status (see Figure S4). As for the Cu^{2+} exchanged sample, an absorption at around 553 nm is observed, corresponding to the incorporated copper species. Note that this absorption intensifies with the increase of exchange times.

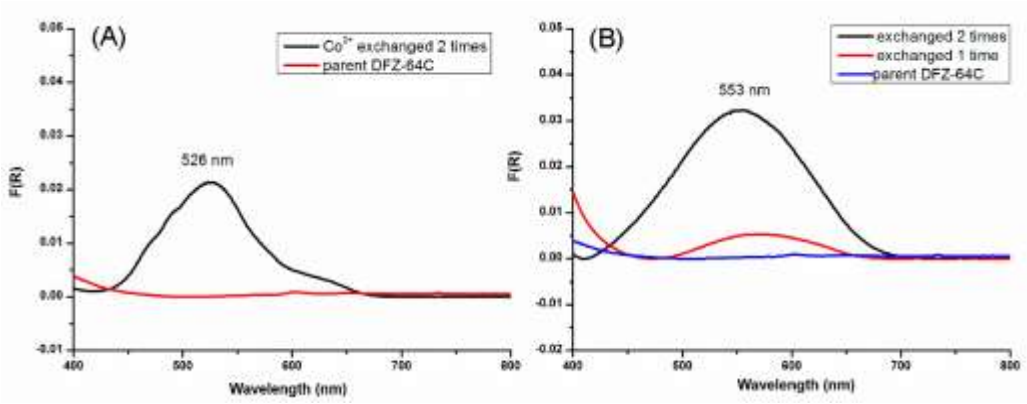

Figure 11 The UV-VIS spectra of sample DFZ-64C after Co^{2+} exchange in 0.05 M $Co(Ac)_2$ solution (A, 50 ºC, 4h) and Cu^{2+} exchange in 0.05 M $Cu(Ac)_2$ solution (B, 50 ºC, 4h).

A.C. Impedance analysis

A. C. impedance spectroscopy is employed to test the ion/proton conductivity of this material at room temperature. The corresponding *a. c*. impedance plots are illustrated in Figure 12. The ion/proton conductivity is calculated to be $1.70*10^{-4}$ S cm^{-1} (293K, 30% relative humidity), which is one magnitude higher than that of a notable open-framework AlPO material JU-103 (around $2.52*10^{-5}$ S cm^{-1}, 293k, 33% relative humidity)[30]. As revealed by the previous structure analysis, abundant Cs^{+} ions, physically adsorbed water and terminal P-OH exist in the structure, which might have endowed the material with this high ion/proton conductivity.

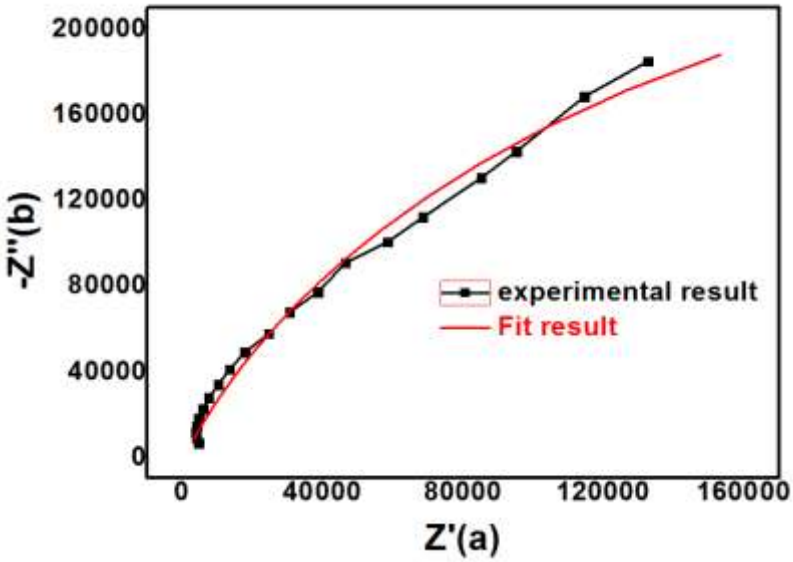

Figure 12 A.C. impedance plots of sample DFZ-64C.

Conclusions

In summary, an open-framework SAPO material with the chemical formula of $Cs_2(Al_{0.875}Si_{0.125})_4(P_{0.875}Si_{0.125}O_4)_4(HPO_4)$ was successfully synthesized in a cesium-containing hydrogel system. The material was resolved to be isostructural with an open-framework aluminophosphate (AlPO) material AlPO-CJ19. This is the first report of the successful synthesis of the silicon-containing counterpart of AlPO-CJ19. The incorporation of the Si species could be testified by both the elemental analysis and the structure analysis. From an environmental point of view, the utilization of pure inorganic synthesis gel makes the current synthesis protocol more favorable. Besides, the thermal stability of the material is significantly improved due to the substitution of the organic template by inorganic Cs^+ cations. UV-vis results reveal that cobalt and copper cations could be readily incorporated through simple ion-exchange treatment. The conductivity of the material is revealed to $1.70*10^{-4}$ S cm^{-1} (293K, 30% relative humidity) as revealed by the A.C. impedance spectroscopy analysis, an impressive value for this kind of

material. The abundant Cs^+ cations and terminal P-OH in this material are the origin of its high ion/proton conductivity.

Conflicts of interest

There are no conflicts of interest to declare.

Acknowledgement

The authors acknowledge funding support from the Sino-French joint laboratory “Zeolites”..

REFERENCES

1. Wilson, S. T.; Lok, B. M.; Messina, C. A.; Cannan, T. R.; Flanigen, E. M., Aluminophosphate Molecular-Sieves - a New Class of Microporous Crystalline Inorganic Solids. *J Am Chem Soc* **1982,** *104* (4), 1146-1147.

2. Mintova, S.; Mo, S.; Bein, T., Nanosized AlPO4-5 molecular sieves and ultrathin films prepared by microwave synthesis. *Chem Mater* **1998,** *10* (12), 4030-4036.

3. Fan, D.; Tian, P.; Su, X.; Yuan, Y. Y.; Wang, D. H.; Wang, C.; Yang, M.; Wang, L. Y.; Xu, S. T.; Liu, Z. M., Aminothermal synthesis of CHA-type SAPO molecular sieves and their catalytic performance in methanol to olefins (MTO) reaction. *J Mater Chem A* **2013,** *1* (45), 14206-14213.

4. Tian, P.; Wei, Y. X.; Ye, M.; Liu, Z. M., Methanol to Olefins (MTO): From Fundamentals to Commercialization. *Acs Catal* **2015,** *5* (3), 1922-1938.

5. Yu, J. H.; Xu, R. R., Insight into the construction of open-framework aluminophosphates. *Chem Soc Rev* **2006,** *35* (7), 593-604.

6. Yu, J. H.; Xu, R. R., Rich structure chemistry in the aluminophosphate family. *Accounts Chem Res* **2003,** *36* (7), 481-490.

7. Yu, J. H.; Li, L. Y.; Xu, R. R., Towards rational design and synthesis of aluminophosphates with 2-D layer and 3-D open-framework structures. *Micropor Mesopor Mat* **2001,** *48* (1-3), 47-56.

8. Yan, W. F.; Yu, J. H.; Xu, R. R.; Zhu, G. S.; Xiao, F. S.; Han, Y.; Sugiyama, K.; Terasaki, O., [Al12P13O52](3-)[(CH2)(6)N4H3](3+): An anionic aluminophosphate molecular sieve with Bronsted acidity. *Chem Mater* **2000,** *12* (9), 2517-2519.

9. Wang, K. X.; Yu, J. H.; Shi, Z.; Miao, P.; Yan, W. F.; Xu, R. R., Synthesis and characterization of a new three-dimensional aluminophosphate [Al11P12O48][C4H12N2][C4H11N2] with an Al/P ratio of 11 : 12. *J Chem Soc Dalton* **2001,** (12), 1809-1812.

10. Fan, D.; Tian, P.; Xu, S. T.; Wang, D. H.; Yang, Y.; Li, J. Z.; Wang, Q. Y.; Yang, M.; Liu, Z. M., SAPO-34 templated by dipropylamine and diisopropylamine: synthesis and catalytic performance in the methanol to olefin (MTO) reaction. *New J Chem* **2016,** *40* (5), 4236-4244.

11. Cundy, C. S.; Cox, P. A., The hydrothermal synthesis of zeolites: History and development from the earliest days to the present time. *Chem Rev* **2003,** *103* (3), 663-701.

12. Tong, X. Q.; Xu, J.; Wang, C.; Lu, H. Y.; Huang, P.; Yan, W. F.; Yu, J. H.; Deng, F.; Xu, R. R., Molecular engineering of microporous crystals: (V) Investigation of the structure-directing ability of piperazine in forming two layered aluminophosphates. *Micropor Mesopor Mat* **2012,** *155*, 153-166.

13. Lu, H. Y.; Tong, X. Q.; Yan, Y.; Yan, W. F.; Yu, J. H.; Xu, R. R., Synthesis, Structure and Phase Transition of a New Microporous Aluminophosphate [C4N2H14](2+)[H2Al3P3O14](2-). *Chem J Chinese U* **2013,** *34* (7), 1571-1575.

14. Awala, H.; Gilson, J. P.; Retoux, R.; Boullay, P.; Goupil, J. M.; Valtchev, V.; Mintova, S., Template-free nanosized faujasite-type zeolites. *Nat Mater* **2015,** *14* (4), 447-451.

15. Ghrear, T. M. A.; Rigolet, S.; Daou, T. J.; Mintova, S.; Ling, T. C.; Tan, S. H.; Ng, E. P., Synthesis of Cs-ABW nanozeolite in organotemplate-free system. *Micropor Mesopor Mat* **2019,** *277*, 78-83.

16. Zhang, H. Y.; Yang, C. G.; Zhu, L. F.; Meng, X. J.; Yilmaz, B.; Muller, U.; Feyen, M.; Xiao, F. S., Organotemplate-free and seed-directed synthesis of levyne zeolite. *Micropor Mesopor Mat* **2012,** *155*, 1-7.

17. Xie, B.; Song, J. W.; Ren, L. M.; Ji, Y. Y.; Li, J. X.; Xiao, F. S., Organotemplate-free and fast route for synthesizing Beta zeolite. *Chem Mater* **2008,** *20* (14), 4533-4535.

18. Iyoki, K.; Itabashi, K.; Okubo, T., Seed-Assisted, One-Pot Synthesis of Hollow Zeolite Beta without Using Organic Structure-Directing Agents. *Chem-Asian J* **2013,** *8* (7), 1419-1427.

19. Yang, C. G.; Ren, L. M.; Zhang, H. Y.; Zhu, L. F.; Wang, L.; Meng, X. J.; Xiao, F. S., Organotemplate-free and seed-directed synthesis of ZSM-34 zeolite with good performance in methanol-to-olefins. *J Mater Chem* **2012,** *22* (24), 12238-12245.

20. Zhang, L.; Yang, C. G.; Meng, X. J.; Xie, B.; Wang, L.; Ren, L. M.; Ma, S. J.; Xiao, F. S., Organotemplate-Free Syntheses of ZSM-34 Zeolite and Its Heteroatom-Substituted Analogues with Good Catalytic Performance. *Chem Mater* **2010,** *22* (10), 3099-3107.

21. Wu, Z. F.; Song, J. W.; Ji, Y. Y.; Ren, L. M.; Xiao, F. S., Organic template-free synthesis of ZSM-34 zeolite from an assistance of zeolite L seeds solution. *Chem Mater* **2008,** *20* (2), 357-359.

22. Zhang, H. Y.; Guo, Q.; Ren, L. M.; Yang, C. G.; Zhu, L. F.; Meng, X. J.; Li, C.; Xiao, F. S., Organotemplate-free synthesis of high-silica ferrierite zeolite induced by CDO-structure zeolite building units. *J Mater Chem* **2011,** *21* (26), 9494-9497.

23. Ng, E. P.; Chateigner, D.; Bein, T.; Valtchev, V.; Mintova, S., Capturing Ultrasmall EMT Zeolite from Template-Free Systems. *Science* **2012,** *335* (6064), 70-73.

24. Ng, E. P.; Awala, H.; Ghoy, J. P.; Vicente, A.; Ling, T. C.; Ng, Y. H.; Mintova, S.; Adam, F., Effects of ultrasonic irradiation on crystallization and structural properties of EMT-type zeolite nanocrystals. *Mater Chem Phys* **2015,** *159*, 38-45.

25. Davis, M. E., Zeolites from a Materials Chemistry Perspective. *Chem Mater* **2014,** *26* (1), 239-245.

26. Meng, X. J.; Xiao, F. S., Green Routes for Synthesis of Zeolites. *Chem Rev* **2014,** *114* (2), 1521-1543.

27. Wang, Y. Q.; Wu, Q. M.; Meng, X. J.; Xiao, F. S., Insights into the Organotemplate-Free Synthesis of Zeolite Catalysts. *Engineering-Prc* **2017,** *3* (4), 567-574.

28. Park, S. H.; Choi, W.; Choi, H. J.; Hong, S. B., Organic-Free Synthesis of Silicoaluminophosphate Molecular Sieves. *Angew Chem Int Edit* **2018,** *57* (30), 9413-9418.

29. Barrer, R. M.; Marshall, D. J., CHEMISTRY OF SOIL MINERALS .I. HYDROTHERMAL CRYSTALLISATION OF SOME ALKALINE AL2O3-SIO2-P2O5 COMPOSITIONS. *Journal of the Chemical Society* **1965,** (NOV), 6616-&.

30. Sun, Y. J.; Yan, Y.; Wang, Y. Y.; Li, Y.; Li, J. Y.; Yu, J. H., High proton conduction in a new alkali metal-templated open-framework aluminophosphate. *Chem Commun* **2015,** *51* (45), 9317-9319.

31. Mu, Y.; Wang, Y. Y.; Li, Y.; Li, J. Y.; Yu, J. H., Organotemplate-free synthesis of an open-framework magnesium aluminophosphate with proton conduction properties. *Chem Commun* **2015,** *51* (11), 2149-2151.

32. Wang, Y. Y.; Sun, Y. J.; Mu, Y.; Zhang, C. Q.; Li, J. Y.; Yu, J. H., Organotemplate-free hydrothermal synthesis of an aluminophosphate molecular sieve with AEN zeotype topology and properties of its derivatives. *Chem Commun* **2014,** *50* (97), 15400-15403.

33. Flanigen, E. M.; Grose, R. W., Phosphorus Substitution in Zeolite Frameworks. In *Molecular Sieve Zeolites-I*, AMERICAN CHEMICAL SOCIETY: 1974; Vol. 101, pp 76-101.

34. Zhou, D.; Chen, L.; Yu, J. H.; Li, Y.; Yan, W. F.; Deng, F.; Xu, R. R., Synthesis, crystal structure, and solid-state NMR Spectroscopy of a new open-framework aluminophosphate (NH4)(2)Al-4(PO4)(4)(HPO4)center dot H2O. *Inorg Chem* **2005,** *44* (12), 4391-4397.

35. Malicki, N.; Mafra, L.; Quoineaud, A. A.; Rocha, J.; Thibault-Starzyk, F.; Fernandez, C., Multiplex MQMAS NMR of quadrupolar nuclei. *Solid State Nucl Mag* **2005,** *28* (1), 13-21.

36. Amoureux, J. P.; Fernandez, C.; Steuernagel, S., Z filtering in MQMAS NMR. *J Magn Reson Ser A* **1996,** *123* (1), 116-118.

37. Louer, D.; Boultif, A., Indexing with the successive dichotomy method, DICVOL04. *Z Kristallogr* **2006**, 225-230.

38. Petricek, V.; Dusek, M.; Palatinus, L., Crystallographic Computing System JANA2006: General features. *Z Krist-Cryst Mater* **2014,** *229* (5), 345-352.

39. Dusek, M.; Petricek, V.; Palatinus, L., Advances in solution of modulated structures reflected by Jana system. *6th International Conference on Aperiodic Crystals (Aperiodic'09)* **2010,** *226*.

40. Kurtz, S. K.; Perry, T. T., A Powder Technique for the Evaluation of Nonlinear Optical Materials. *Journal of Applied Physics* **1968,** *39* (8), 3798-3813.

41. Palatinus, L.; Chapuis, G., SUPERFLIP - a computer program for the solution of crystal structures by charge flipping in arbitrary dimensions. *J Appl Crystallogr* **2007,** *40*, 786-790.

42. Brown, I. D., VALENCE: A program for calculating bond valences. *J Appl Crystallogr* **1996,** *29*, 479-480.

43. Brese, N. E.; Okeeffe, M., Bond-Valence Parameters for Solids. *Acta Crystallogr B* **1991,** *47*, 192-197.

44. Stephens, P., Phenomenological model of anisotropic peak broadening in powder diffraction. *J Appl Crystallogr* **1999,** *32* (2), 281-289.